Int. J. Electrochem. Sci., 16 **(2021)** Article ID: 210235, doi: 10.20964/2021.02.13

International Journal of
ELECTROCHEMICAL
SCIENCE
www.electrochemsci.org

Short Communication

Electrochemical and Optical Properties of Tellurium Dioxide (TeO_2) Nanoparticles

Abdelfattah Amari[1,2], Mohammed K. Al Mesfer[1], Norah Salem Alsaiari[3], Mohd Danish[1,4], Ali M. Alshahrani[5], Mohamed A. Tahoon[5,6], and Faouzi Ben Rebah[5,7]*

[1] Department of Chemical Engineering, College of Engineering, King Khalid University, PO Box 9004, Abha 61413, Saudi Arabia
[2] Research Laboratory: Energy and Environment, National School of Engineers, Gabes University, Gabes 6072, Tunisia
[3]Chemistry Department, College of Science, Princess Nourah Bint Abdulrahman University, Riyadh, Saudi Arabia
[4] Chemical Engineering Department, Indian Institute of Technology, Roorkee, India
[5] Department of Chemistry, College of Science, King Khalid University, P.O. Box 9004, Abha 61413, Kingdom of Saudi Arabia
[6] Chemistry Department, Faculty of Science, Mansoura University, 35516 Mansoura, Egypt
[7] Higher Institute of Biotechnology of Sfax (ISBS), Sfax University, P.O. Box 263, Sfax 3000, Tunisia
[*]E-mail: tahooon_87@yahoo.com

Received: 21 September 2020 / *Accepted:* 15 November 2020 / *Published:* 31 December 2020

Herein, a facile hydrothermal method was used for the preparation of nanostructured TeO_2. Different techniques (X-ray diffraction, transmission electron microscope, and scanning electron microscope) were used for morphology, size, and crystalline structure identification of synthesized TeO_2 nanoparticles. Fourier transform infrared and ultraviolet-visible spectroscopies were used for optical properties characterization of nanoparticles. Nanostructured TeO_2 having a spherical and uniform shape and particle size ~12 nm that approved via transmission electron microscope. TeO_2/ITO glass electrode was fabricated in order to study the electrochemical properties by using cyclic voltammetry and electrochemical impedance spectroscopy. Electrochemical measurements of the fabricated TeO_2/indium tin oxide electrode showed that the electrode having excellent sensitivity. Thus, the TeO_2 nanoparticles can further used for biosensors applications.

Keywords: Tellurium oxide; Nanoparticles; Optical properties; Synthesis and characterization

1. INTRODUCTION

We have done this research as an extension of our work previously published in other journals [1-11]. Many new applications in different areas have been opened in recent years due to the

preparation of nanostructured materials. Materials show unique properties when their size reduces to nanoscale that couldn't show by their bulk and these properties are known to be rich for new scientific developments. Semimetal oxide nanoparticles are a class of nanostructured materials with novel properties that allow its use in many applications like catalysis [12], fuel cell [13], gas sensing [14], and the medical field [15]. At room temperature, tellurium is a semimetal of p-type with 0.35 eV narrow bandgap [16]. As important semimetal materials, Te based compounds have exceptional properties like thermoelectric properties, non-linear optical response, and photoconductivity that make Te an important substance for manufacturing optical-electronic devices [17-19]. Te is also used as a useful material for heavy metals removal [20], gas sensors for NO_2, and CO [21, 22] and manufacturing of photoconductors [23]. Te nanoparticles are prepared by different techniques like microwave [24], electrochemical deposition [25], and hydrothermal methods [26]. Te nanoparticles are prepared in different shapes as nanorods [27], and nanotubes [28]. Also, wet chemistry is recently used for the preparation of Te nanoparticles [29, 30]. Chemical routes of TeO_2 nanoparticles preparation are involved thermal oxidation of Te micro-tubes [31], sol-gel, [32] and thermal evaporation of Te microstructures [33]. So, the preparation of these nanomaterials required more trials for investigations. Here, nanostructured TeO_2 was synthesized by using $TeCl_4$ as a precursor of tellurium. The method used is the facile hydrothermal route in which TeO_2 is produced and characterized by using a scanning electron microscope (SEM), X-ray diffraction (XRD), Fourier transform infrared spectroscopy (FTIR), and UV-visible spectroscopy. The electrochemical performance of the prepared nanostructured TeO_2 is investigated. It is observed that the synthesized TeO_2 nanostructures have a wide application in the biomedical fields.

2. EXPERIMENTAL SECTION

2.1. Materials

Ethanol (EtOH), polyethylene glycol (PEG-6000), $TeCl_4$, and sodium dodecyl sulfate (SDS) were purchased from India (Oxford Co.). All used chemicals were analytical grade and used as received without further purification. Glass sheets of resistance 16Ω/cm (Balzers) coated with hydrolyzed indium tin oxide (ITO) was used for the loading of TeO_2 film and tested as a working electrode.

2.2. Synthesis of TeO_2 nanoparticles

The perfect synthesis of TeO_2 nanoparticles is beginning by dissolving 0.1 g $TeCl_4$ with 0.007 g SDS or PEG as a surfactant in 40 ml of distilled water at room temperature with continuous stirring for 7 min. Then, at 200 ^{O}C all reagents were kept in the autoclave for 8 h and after that permitted to cool down at room temperature. With absolute ethanol and distilled water, the isolated precipitate by centrifuging was washed several times and then dried at 70 ^{O}C for 5h. Then the sample was annealed for one hour at 400 ^{O}C.

2.3. TeO_2/ITO electrode fabrication

For the preparation of the TeO_2/ITO electrode, the prepared TeO_2 was dissolved in de-ionized water. TeO_2 solution was sonicated for a half-hour to completely disperse of nanostructured TeO_2 before the electrophoretic deposition process as shown in Scheme 1. The fabricated electrode surface area is 0.26 cm^2 obtained by optimizing the time and potential of electrophoretic deposition at 45 s and 40 V respectively.

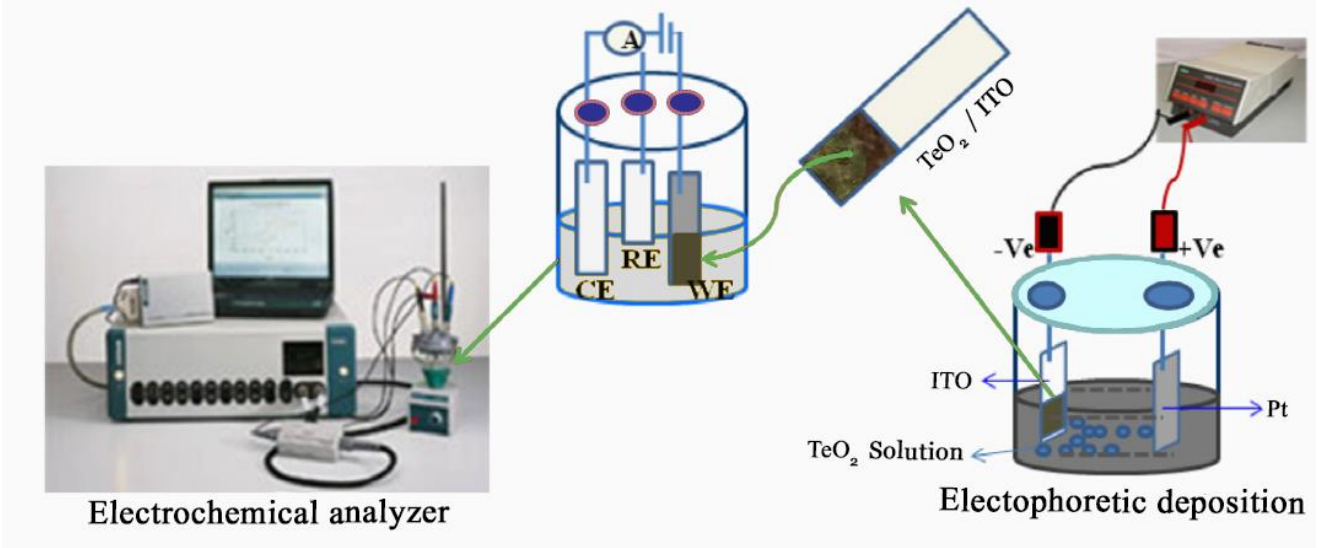

Scheme 1. Schematic representation for the fabrication of TeO_2/ITO electrode for electrochemical studies.

3. RESULTS AND DISCUSSION

3.1. X-ray diffraction of nanostructured TeO_2

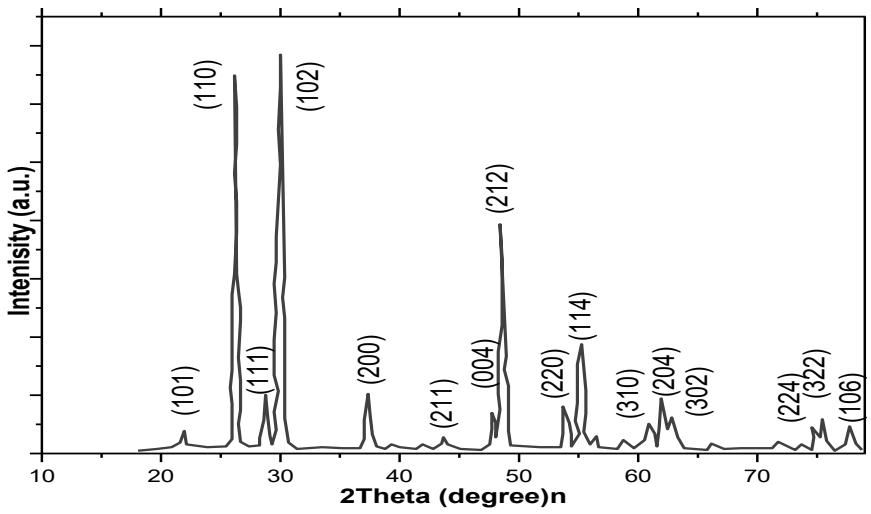

Figure 1. XRD of the nanostructured TeO_2 synthesized by hydrothermal method

Fig. 1 shows the X-ray diffraction pattern of nanostructured TeO_2. The diffraction peaks parallel to the tetragonal phase of TeO_2 (JCPDS 76-0679). No peaks parallel to any impurities are identified in the obtained X-ray peaks that indicate the presence of the single-crystalline phase of TeO_2. The excellent crystallinity of synthesized nanostructured TeO_2 is also indicated by sharp and strong peaks.

The average crystal size (d) can be calculated by using the Debye Scherrer equation as shown in Eq.1. The average size of nanostructured TeO_2 is found to be ~ 12 nm.

$$d = \frac{0.9\,\lambda}{\beta COS\theta} \quad (1)$$

Each symbol of the equation has its well-known meaning. As described elsewhere, θ is the glancing angle, β is calculated from diffraction peaks as the width of half maxima and λ is the wavelength of X-ray that equal 1.5 Å.

3.2. Transmission Electron Microscope (TEM) and Scanning Electron Microscope (SEM)

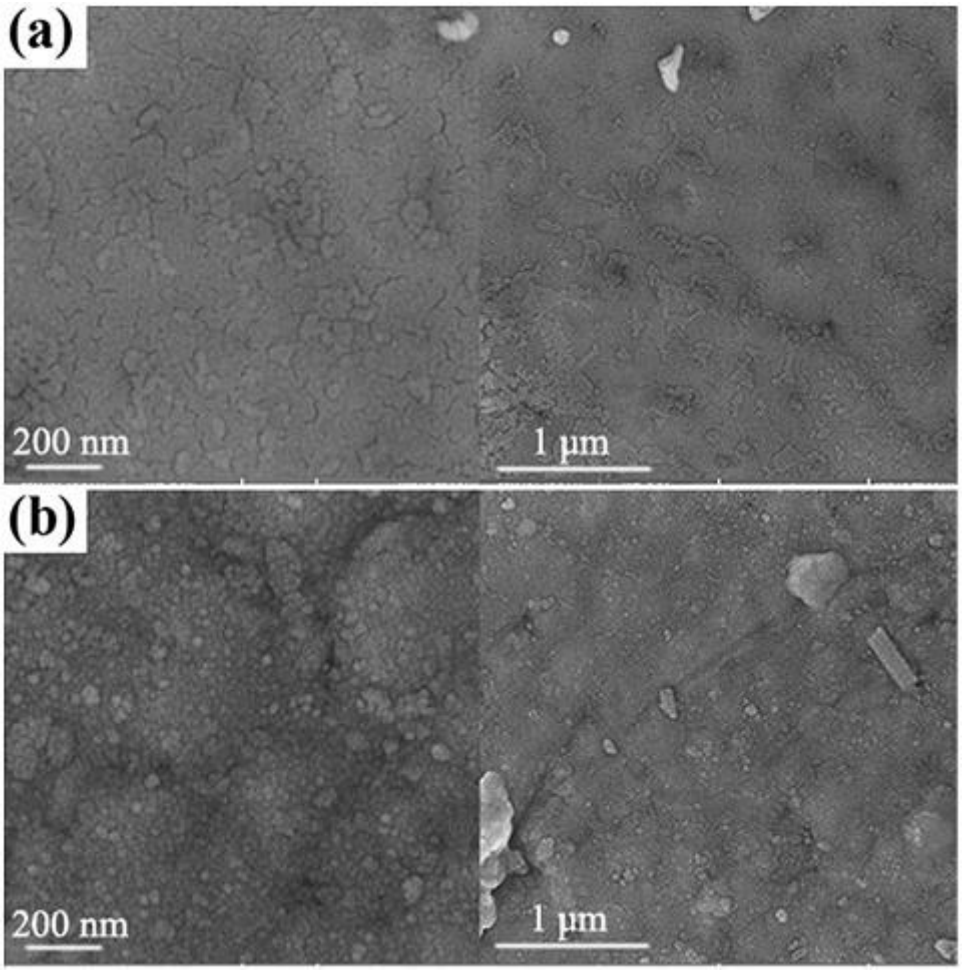

Figure 2. SEM images of nanostructured TeO_2 in case of using (a) SDS and (b) PEG surfactants

Fig. 2 shows the scanning electron microscope image of the prepared nanostructured TeO_2 by using SDS and PEG as a surfactant. SEM image illustrates a spherical shape of the prepared

nanoparticles. Also, the SEM image shows uniformly distributed morphology of the nanostructured TeO_2. The morphology of the particles is not affected by changing the used surfactant from SDS to PEG.

The size of particles is affected by changing the surfactant. In the case of using neutral PEG, the size of particles is appeared to be larger compared to using SDS. The transmission electron microscope image is shown in Fig. 3. The TEM image of prepared TeO_2 nanoparticles approves the spherical morphology of prepared particles as appeared in the SEM results. As shown in the TEM image the particle size appeared to be 10-20 nm which approves the results of XRD.

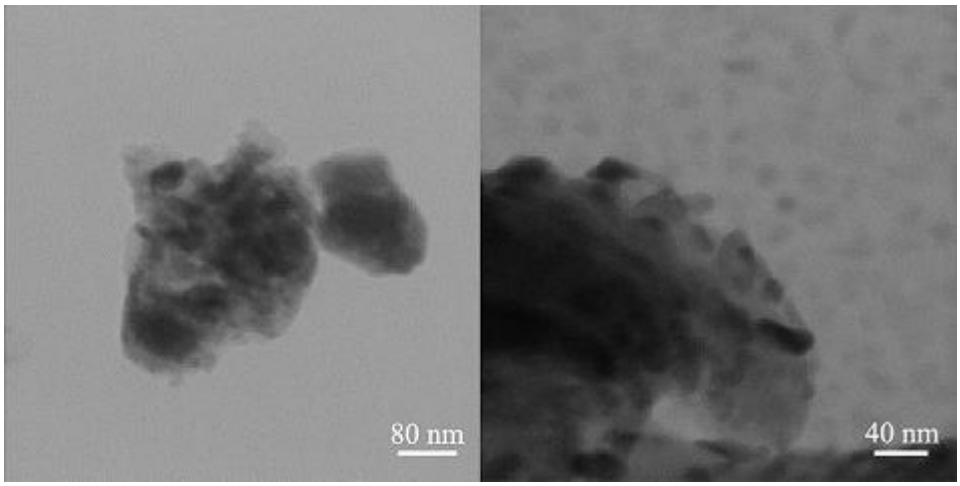

Figure 3. TEM images of nanostructured TeO_2

3.3. Fourier transform infrared and ultraviolet-visible studies

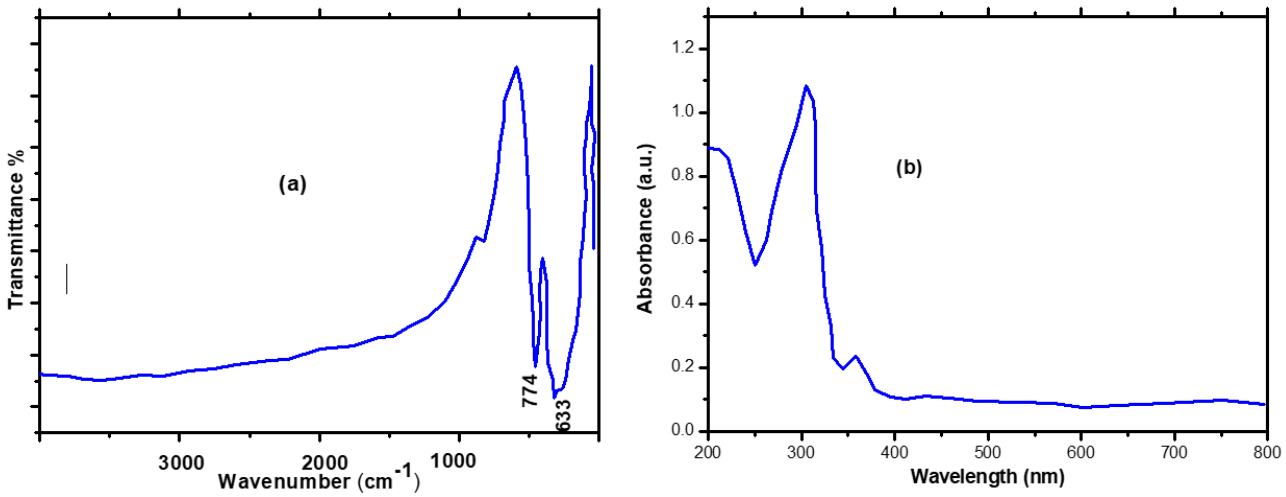

Figure 4. FT-IR spectra (a) and UV-visible spectra (b) of prepared TeO_2 nanoparticles.

As it is considered a powerful tool for the characterization of material structure, the Fourier transform infrared and ultraviolet-visible spectroscopy are used for the characterization of prepared nanostructured TeO_2. The Fourier transform infrared and ultraviolet-visible spectroscopy of prepared

TeO_2 is shown in Fig. 4. FT-IR of nanostructured TeO_2 shows two absorption bands at 774 and 663 cm^{-1}. The two bands are considered to be the vibrations of Te-O bonds.

The appeared two bands are similar to the α-TeO_2 [34] which approves the preparation of α-TeO_2 crystalline structure. The absence of impurities is observed by the absence of any other peaks in FT-IR spectra. UV-Vis absorption spectroscopy is a powerful tool for optical properties characterization. UV-Vis absorption spectroscopy of prepared nanostructured TeO_2 is shown in Fig.4. When conjugated with a proper n-type semiconductor, TeO_2 can be used for solar cell construction as it is a p-type semiconductor. UV-Vis absorption spectroscopy of nanostructured TeO_2 is determined in the range of 200-800 nm. From Fig. 4, TeO_2 exhibits one absorption peak at 300 nm due to the transition from the valence band to the conduction band [30]. According to the UV-Vis absorption spectrum of TeO_2 nanoparticles, TeO_2 nanoparticles can be used for the fabrication of optoelectronic devices. Also, TeO_2 is a p-type semiconductor and can be conjugated with an n-type semiconductor and used for the fabrication of optical devices as photovoltaic devices and p–n junction photodiode [35-37].

3.4. Electrochemical studies

3.4.1. Scan rate effect

The effect of varying scan rate on the fabricated TeO_2/ITO electrode at the range of 10 - 100 mVs^{-1} was performed by using the cyclic voltammetry technique as shown in Fig. 5. The used electrolytic solution consisted of phosphate buffer, saline 50 mM, and 5mM ferricyanide $[Fe(CN)_6]^{3/4}$. As shown in Fig.5, the anodic and cathodic peak currents (E_{pa}, E_{pc}) and potential peak separation (ΔE_p) are increased linearly with the square root of the scan rate $\nu^{1/2}$ suggesting that the electrochemical process is diffusion-controlled electron transfer process [38-41] as electrons are migrated from TeO_2/ITO electrode redox centers. The excellent electro-catalytic performance of the fabricated TeO_2/ITO is indicated by the linear dependence of peak current with the scan rate in which the linear correlation R^2=0.998 and standard deviation of 2.6 $X10^{-4}$ [42-46]. A well-defined oxidation peak is observed in Fig. 5 due to the electron transfer between TeO_2/ITO electrode surface and electrolyte. Both anodic (E_{pa}) and cathodic (E_{pc}) peak potential shift linearly towards the higher side with the increase in scan rate. This relationship confirms the irreversible or slow electron transfer kinetics between the TeO_2/ITO electrode and electrolyte [47]. The advantage of maximum redox current of TeO_2/ITO film is to enhance the sensitivity of electronic devices like biosensor for biomedical applications [48-54].

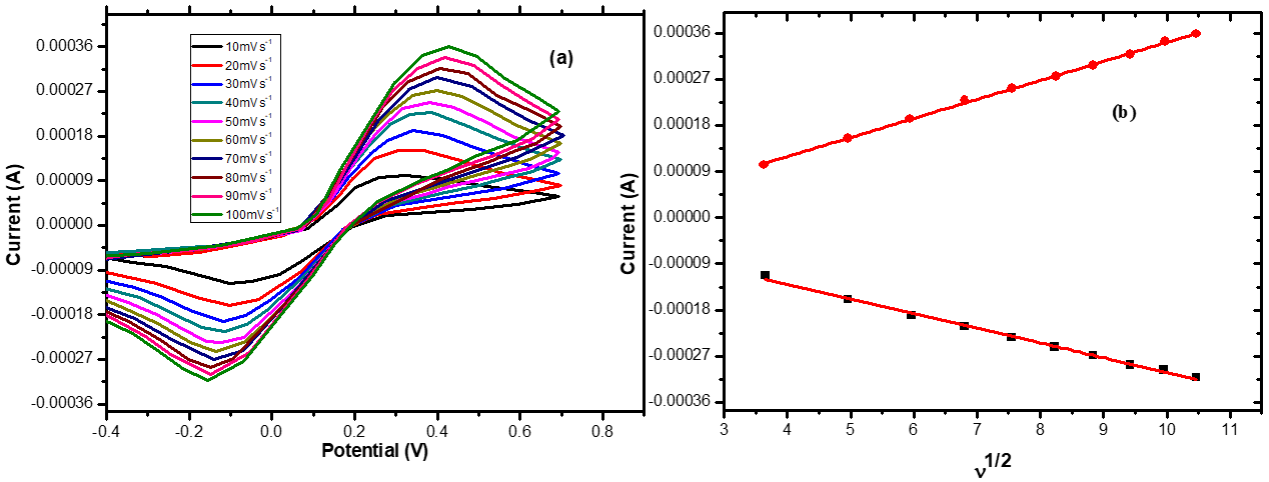

Figure 5. Cyclic voltammogram of TeO_2/ITO electrode at scan rate 10-100mVs^{-1} in phosphate buffer saline (PBS) and (50 mM 0.9% NaCl) containing $[Fe(CN)_6]^{3/4}$ 5 mM as the mediator (a) and cathodic and anodic current vs √ν (scan rate square root) at scan rate 10-100 mVs^{-1} (b)

The formation of water-soluble tellurium species leads to the leaching out of more than 80% of the electrode surface after ten cycles making the redox peaks of tellurium unstable.

3.4.2. Electrochemical impedance spectroscopy

The resistance of the fabricated TeO_2/ITO electrode can be more understood by performing the electrochemical impedance spectroscopy in the same electrolytic solution of cyclic voltammetry (phosphate buffer, saline 50 mM, and 5 mM ferricyanide $[Fe(CN)_6]^{3-/4-}$) at a time of 5-25 s, scan rate 0.25-2.5 mV, and frequency 0-1.2X10^5 Hz. The Nyquist plots are shown in Fig.6a that consists of two parts, a semicircle part followed by a straight part. Fig. 6 shows the electron transfer process at the semicircle part (high frequency). The diameter of the semicircle part is corresponding to the charge transfer resistance (Rct) that decreases linearly with time as shown in Fig. 6 from 5 to 25 s (Rct5s = 5.20 kΩ > Rct10s = 4.95 kΩ > Rct15s = 4.53 kΩ > Rct20s = 4.26 kΩ > Rct25s = 4.14 kΩ) for the fabricated electrode as a result of the diffusion limiting step of the electrochemical reaction. Thus, the fabricated electrode provides a long time for the electron transfer process between electrode and solution as well as providing an easier electron transfer process due to the presence of a small and hydrophilic surface layer. The results are approved by the decrease of charge transfer resistance by increasing the scan rate as shown in Fig. 6.

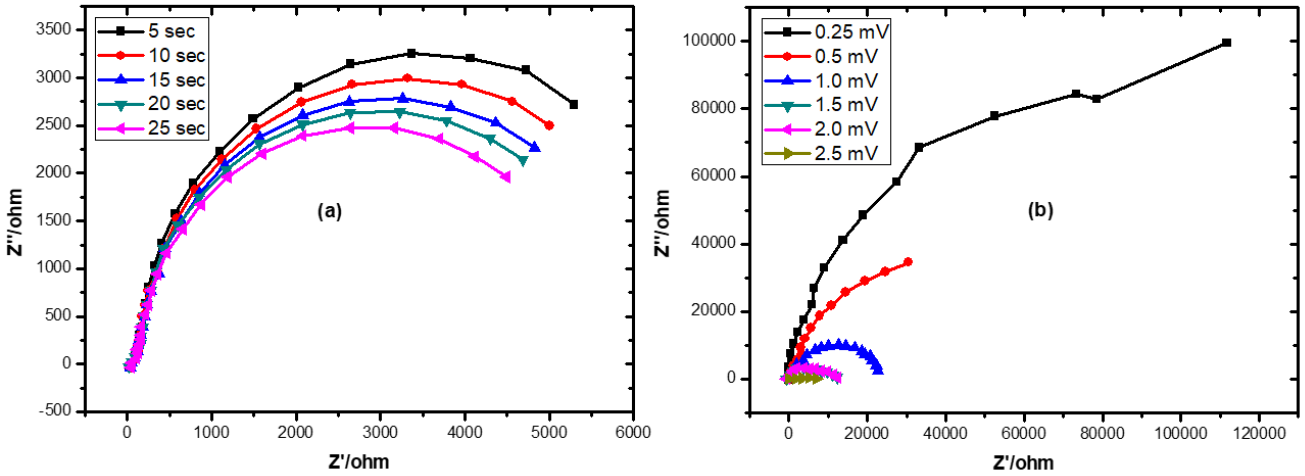

Figure 6. Nyquist plot as a function of scan rate at different times in phosphate buffer (50 mM, pH 7.0, 0.9% NaCl) containing 5 mM $[Fe(CN)_6]^{3/4}$ (a), and with a function of voltage scan rate (b)

Long term pathway among electrolyte and electrode is the main reason for the decrease. Fig. 6b shows the Nyquist plots measured at different voltage scan rate in the range of (0.25–2.5 mV). According to the figure, the value of charge transfer resistance decreases with increasing the voltage scan rate due to the high electron pathways between the electrode and electrolyte, resulting an improved diffusion of ferricyanide towards the surface of TeO_2/ITO electrode [55, 56]. So, the presence of TeO_2 nanoparticles causes a limitation in the charge transfer process that affects the electrochemical behavior of the prepared electrode [37].

4. CONCLUSION

In summary, $TeCl_4$ was used as a tellurium source for the preparation of nanostructured TeO_2 by a facile hydrothermal method. The synthesized nanoparticles were characterized using XRD, TEM, and SEM. The optical properties were determined using FT-IR spectra and UV-visible spectroscopy. In addition, TeO_2 nanoparticles were precipitated on the ITO glass electrode for electrochemical properties determination. Moreover, the cyclic voltammetry study reveals that TeO_2 nanoparticles exhibit excellent charge transferability due to its nature that helps the electron transfer during the electrochemical process. So, specific optical and electrochemical properties are approved for TeO_2 nanoparticles. Thus, nanostructured TeO_2 reveals specific properties that enhance its use in multi applications like bioelectronics devices, biosensors, and semiconducting devices.

ACKNOWLEDGEMENTS
The authors extend their appreciation to the Deanship of Scientific Research at King Khalid University for funding this work through research groups program under grant number R.G.P.2/96/41. Also, this research was funded by the Deanship of Scientific Research at Princess Nourah bint Abdulrahman University through the Fast-track Research Funding Program.

References

1. E. A. Gomaa, A. Negm, and M. A. Tahoon, *J. Taibah Univ. Sci*., 11 (2017) 741.
2. E. A. Gomaa, M. A. Tahoon, and A. Negm, *J. Mol. Liq*., 241 (2017) 595.
3. E. A. Gomaa, and M. A. Tahoon, *J. Mol. Liq*., 214 (2016) 19.
4. E. A. Gomaa, M. A. Tahoon, and A. Shokr, *J. Chemical Data Collections*, 3-4 (2016) 58.
5. M. A. Tahoon, E. A. Gomaa, and M. H. A. Suleiman, *open chemistry*, 17 (2019) 260.
6. S. M. Siddeeg, M. A. Tahoon, and F. B. Rebah, *Materials Research Express*, 7 (2019) 012001.
7. F. Ben Rebah, S. M. Siddeeg, and M. A. Tahoon, *Egyptian Journal of Chemistry*, 62 (2019) 393.
8. S. M. Siddeeg, M. A. Tahoon, and F. B. Rebah, *Processes*, 7 (2019) 800.
9. S. M. Siddeeg, M. A. Tahoon, W. Mnif, and F. B. Rebah, *Processes*, 8 (2020) 5.
10. S. M. Siddeeg, A. Amari, M. A. Tahoon, N. S. Alsaiari, and F. B. Rebah, *Alexandria Engineering Journal*, 59 (2020) 905.
11. M. A. Tahoon, S. M. Siddeeg, N. S. Alsaiari, W. Mnif, and F. B. Rebah, *Processes*, 8 (2020) 645.
12. E. N. Voskresenskaya, L. I. Kurteeva, and A. G. Anshits, *Appl. Catal., A: General*, 90 (1992) 209.
13. J. C. Boivin, *Int. J. Inorg. Mater*., 3 (2001) 1261**.**
14. A. Cabot, A. Marsal, J. Arbiol, and J. R. Morante, *Sens. Actuators* B, 99 (2004) 74.
15. E. Kanazawa, G. Sakai, K. Shimanoe, Y. Kanmura, Y. Teraoka, N. Miura, and N. Yamazoe, *Sens. Actuators B*, 77 (2001) 72.
16. M. Panahi-Kalamuei, M. Mousavi-Kamazani, and M. Salavati-Niasari, *Mater. Lett*., 136 (2014) 218.
17. C. S. S. Sandeep, A. K. Samal, T. Pradeep, and R. Philip, *Chem. Phys. Lett*., 485 (2010) 326.
18. K. Sridharan, V. Tamilselvan, D. MYuvaraj, K. N. Rao, and R. Philip, *Opt. Mater*., 34 (2012) 639.
19. J. Wang, X. Zhang, R. Ke, S. Zhang, C. Mao, H. Niu, J. Song, S. Li, and Y. Tian, *Semicond. Sci. Technol*., 31 (2016) 055011.
20. T. Y. Wei, H. Y. Chang, and C. C. Huang, *RSC Adv.*, 3 (2013), 13983.
21. D. Tsiulyanu, S. Marian, and H. D. Liess, *Sens. Actuators* B, 85 (2002), 232.
22. T. Siciliano, E. Filippo, A. Genga, G. Micocci, M. Siciliano, and A. Tepore, *Sens. Actuators* B, 142 (2009) 185.
23. Y. Wang, Z. Tang, P. Podsiadlo, Y. Elkasabi, J. Lahann, and N. Kotov, *Adv. Mater*., 18 (2006) 518.
24. Y. J. Zhu, W. W. Wang, R. J. Qi, and X. L. Xu, *Angew. Chem., Int. Ed*., 43 (2004) 1410.
25. A. W. Zhao, C. H. Ye, G. W. Meng, L. D. Zhang, and P. M. Ajayan, *J. Mater. Res*., 18 (2003) 2318.
26. M. S. Mo, J. H. Zeng, X. M. Liu, W. C. Yu, S. Y. Zhang, and Y. T. Qian, *Adv. Mater*., 14 (2002) 1658.
27. H. H. Li, P. Zhang, C. L. Liang, J. Yang, M. Zhou, X. H. Lu, and G. A. Hope, *Cryst. Res. Technol*., 47 (2012) 1069.
28. Y. Rheem, C. H. Chang, C. M. Hangarter, D. Y. Park, K. H. Lee, Y. S. Jeong, and N. V. Myung, *Electrochim. Acta*, 55 (2010) 2472.
29. H. Zhu, H. Zhang, J. Liang, G. Rao, J. Li, G. Liu, Z. Du, H. Fan, and J. Luo, *J. Phys. Chem*. C, 115 (2011) 6375.
30. U. K. Gautam, and C. N. R. Rao, *J. Mater. Chem*., 14 (2004) 2530.
31. E. Filippo, T. Siciliano, A. Genga, G. Micocci, M. Siciliano, and M. Tepore, *Appl. Surf. Sci*., 265 *(*2013) 329.
32. H. Y. Wei, J. Lin, W. H. Huang, Z. B. Feng, and D. W. Li, *Mater. Sci. Eng*., B, 164 (2009) 51.
33. Z. Liu, T. Yamazaki, Y. Shen, T. Kikuta, and N. Nakatani, *Jpn. J. Appl. Phys*., 47 (2008) 771.
34. B. Qin, Y. Bai, Y. Zhou, J. Liu, X. Xie, and W. Zheng, *Mater. Lett*. , 63 (2009) 1949.
35. X. Jiang, T. Herricks, and Y. Xia, *Nano Lett*., 2 (2002) 1333.
36. A. S. Zoolfakar, R. A. Rani, A. J. Morfa, S. Balendhran, A. P. O. Mullane, S. Zhuiykov, and K. Kalantar-zadeh, *J. Mater. Chem*., 22 (2012) 21767.
37. Srivastava M., Singh J., Mishra R.K., Ojha A.K., *J. of Alloys and Compounds*, 555 (2013) 123.

38. E. A. Gomaa, A. Negm, and R. M. Abu-Qarn, *Measurement*, 125 (2018) 645.
39. E. A. Gomaa, A. Negm, and M. A. Tahoon, *European Journal of Chemistry*, 7 (2016) 341. https://doi.org/10.5155/eurjchem.7.3.341-346.1471
40. S. M. Siddeeg, N. S. Alsaiari, M. A. Tahoon, and F. B. Rebah, *Int. J. Electrochem. Sci*, 15 (2020) 3327.
41. A. Amari, B. Alalwan, S. M. Siddeeg, M. A. Tahoon, N. S. Alsaiari, and F. B. Rebah, *Int. J. Electrochem. Sci*, 15 (2020) 11427.
42. A. Karthika, V. R. Raja, P. Karuppasamy, A. Suganthi, and M. Rajarajan, *Microchemical Journal*, 145 (2019) 737.
43. D. Ragupathy, J. J. Park, S. C. Lee, J. C. Kim, P. Gomathi, M. K. Kim, S. M. Lee, H. D. Ghim, A. Rajendran, S. H. Lee, and K. M. Jeon, *Macromolecular Research*, 19 (2011) 764.
44. P. M. Jahani, M. Jafari, V. K. Gupta, S. Agarwa, *Int. J. Electrochem. Sci.*, 15 (2020) 6829.
45. A. Azadbakht, A. R. Abbasi, Z. Derikvand, and Z. Karimi, *Nano-Micro Letters*, 7 (2015) 152.
46. G. Shen, Y. Guo, X. Sun, and X. Wang, *Nano-Micro Lett.*, 6 (2014) 143.
47. D. R. Dreyer, S. Park, C. W. Bielawski, and R. S. Ruoff, *Chem. Soc. Rev.*, 39 (2010) 228.
48. R. Kumar, *Nano-Micro Lett.*, 12 (2020) 122.
49. H. Lv, Q. Pan, Y. Song, X.-X. Liu, and T. Liu, *Nano-Micro Lett.*, 12 (2020) 118.
50. S. Balasubramaniam, A. Mohanty, S. K. Balasingam, S. J. Kim, and A. Ramadoss, *Nano-Micro Lett.*, 12 (2020) 85.
51. J. Cheng, L. Gao, T. Li, S. Mei, C. Wang, B. Wen, W. Huang, C. Li, G. Zheng, H. Wang, and H. Zhang, *Nano-Micro Lett.*, 12 (2020) 179.
52. N. Sun, Z. Guan, Q. Zhu, B. Anasori, Y. Gogotsi, and B. Xu, *Nano-Micro Lett.*, 12 (2020) 89.
53. Y. Wang, X. Wang, X. Li, R. Liu, Y. Bai, H. Xiao, Y. Liu, and G. Yuan, *Nano-Micro Lett.*, 12 (2020) 115.
54. Y. Zhan, A. Buffa, L. Yu, Z. J. Xu, and D. Mandler, *Nano-Micro Lett.*, 12 (2020) 141.
55. S. Singal, A. K. Srivastava, and Rajesh, *Nano-Micro Lett.*, 9 (2017) 7.
56. Y. Chen, J. Li, G. Yue, and X. Luo, *Nano-Micro Lett.*, 9 (2017) 32.